# Geometry of the 20 November 2003 magnetic cloud

Katsuhide Marubashi,[1] Kyung-Suk Cho,[1,2,3] Yeon-Han Kim,[1] Yong-Deuk Park,[1] and Sung-Hong Park[1]

[1]   This study is an attempt to find a coherent interpretation of the link between the 20 November 2003 magnetic cloud (MC) and its solar source. Most previous studies agree on the orientation of the MC, but the orientation is nearly perpendicular to the axis of the post-eruption arcade (PEA) or the orientation of the neutral line in the solar source region. We first determine the geometry of this MC by fitting methods with both torus and cylinder models. Three possible geometries are obtained, which can reproduce the observed magnetic field variations associated with the MC, one from the cylinder fit and two from the torus fit. The cylinder fit gives the MC orientation with a tilt of a large angle (~60°) from the ecliptic plane and nearly perpendicular to the PEA axis, being similar to those from previous studies. In contrast, two torus fit results give the MC axis with tilt angles less than 20° from the ecliptic plane. The two torus results correspond to the spacecraft encounter with the eastern flank of the flux rope loop (model A) and the western flank of the loop (model B), respectively. In either case, the orientation of the loop around the apex is nearly parallel to the PEA as observed by the SOHO/extreme ultraviolet imaging telescope instrument in the most plausible solar source region of a halo coronal mass ejection (CME), which appeared in the field of view of Large Angle and Spectrometric Coronagraph (LASCO) C2 at 08:50 UT, 18 November 2003. The magnetic helicity of the PEA region is positive in agreement with the helicity of the MC. The 3-D reconstruction from the Solar Mass Ejection Imager data shows that the main part of the ejected plasma expands mainly to the west of the Sun-Earth line. Thus, we reach the most straightforward interpretation of the link between the MC and its solar source as follows. The MC was created in association with the launch of the CME that was first observed by the LASCO C2 at 08:50 UT, 18 November 2003, and propagated through interplanetary space with its orientation almost unchanged. The spacecraft encountered the eastern flank of the loop as described by model A.

## 1.   Introduction

[2]   The magnetic cloud (MC) of 20 November 2003 has been well studied [*Gopalswamy et al.*, 2005; *Yurchyshyn et al.*, 2005; *Wang et al.*, 2006; *Möstl et al.*, 2008], because it caused the largest geomagnetic storm of solar cycle 23 with a minimum *Dst* value of −422 nT [*Zhang et al.*, 2007]. The central objective of these studies is to understand how the MC was created in the solar corona and how the geometry of the MC could be changed during the propagation from the Sun to the Earth. They all conclude that the MC was created in association with the coronal mass ejection (CME) from the NOAA active region (AR) 10501 on 18 November 2003, which first appeared in the field of view of the Large Angle

and Spectrometric Coronagraph (LASCO) C2 at 08:50 UT. As for the detailed connection between the MC and the CME, however, their conclusions are far from agreement, mainly due to the complexity of AR 10501. In fact, this complexity as well as its high activity during October through November is one of the reasons why this active region has kept drawing so much attention. The structure of the AR is characterized by a large negative-polarity spot, surrounded by weaker positive polarities, with a large U-shaped filament along the polarity inversion line.

[3]   In order to understand the relation between an MC and its solar source event, it is crucial to compare the helicity sign of the MC with the helicity sign of its solar source region and to compare the orientation of the MC with the orientation of the magnetic neutral line in the source region (see the review by *Démoulin* [2008, and references therein]). It is generally accepted that the MC has helical magnetic structure that originates from the helical magnetic structure of the solar source region. Therefore, the signs of the magnetic helicities of the MCs and those of the solar source regions should

[1]Korea Astronomy and Space Science Institute, Daejeon, South Korea.
[2]Also at NASA Goddard Space Flight Center, Greenbelt, Maryland, USA.
[3]Also at Catholic University of America, Washington, D. C., USA.

**Table 1.** MC Parameters Determined by Torus Fitting

| Data ID | $R_M^a$ (AU) | $r_{m_0}^a$ (AU) | $\theta_n^b$ (deg) | $\phi_n^b$ (deg) | $sgn^b$ ($B_x$) | $p_y^c$ ($r_{m_0}$) | $p_z^c$ ($r_{m_0}$) | $p^c$ ($r_{m_0}$) | $B_T^d$ (nT) | $U_{T_0}^e$ (km s$^{-1}$) | $D_f^e$ (km s$^{-1}$ h$^{-1}$) | $H^f$ | $T_0^g$ (h) | $E_{rms}^h$ |
|---|---|---|---|---|---|---|---|---|---|---|---|---|---|---|
| | | | | *ACE (20 Nov 2003 11:00 UT to 21 Nov 2003 00:30 UT)* | | | | | | | | | | |
| A | 0.214 | 0.019 | −72.0 | 142.6 | + | −1.12 | 0.05 | 0.75 | 82.6 | 651 | 9.7 | R | 30 | 0.215 |
| B | 0.156 | 0.032 | −58.8 | 34.2 | − | 0.94 | 0.17 | 0.76 | 79.0 | 641 | 8.1 | R | 23 | 0.165 |
| | | | | *ACE (20 November 2003 11:00 UT to 20 Nov 2003 19:20 UT)* | | | | | | | | | | |
| C | 0.200 | 0.014 | −57.1 | 115.4 | + | −0.85 | −0.38 | 0.83 | 78.7 | 646 | 10.3 | R | 124 | 0.213 |
| D | 0.176 | 0.017 | −40.7 | 69.0 | − | 0.59 | 0.74 | 0.80 | 83.7 | 640 | 8.5 | R | 54 | 0.143 |
| | | | | *Wind (20 Nov 2003 12:00 UT to 21 Nov 2003 02:00 UT)* | | | | | | | | | | |
| A′ | 0.181 | 0.031 | −68.7 | 170.4 | + | −1.16 | 0.35 | 0.66 | 66.8 | 677 | 12.3 | R | 31 | 0.176 |
| B′ | 0.191 | 0.023 | −61.1 | 52.5 | − | 0.98 | 0.31 | 0.75 | 75.5 | 674 | 12.1 | R | 22 | 0.198 |
| | | | | *Wind (20 Nov 2003 12:10 UT to 20 Nov 2003 20:50 UT)* | | | | | | | | | | |
| C′ | 0.294 | 0.014 | −56.3 | 112.8 | + | −0.86 | −0.37 | 0.85 | 73.9 | 687 | 15.8 | R | 73 | 0.174 |
| D′ | 0.228 | 0.015 | −46.6 | 69.3 | − | 0.71 | 0.62 | 0.85 | 75.6 | 672 | 12.9 | R | 51 | 0.191 |

[a]$R_M$ is the major radius of torus (constant), and $r_{m_0}$ is the minor radius of torus at the time of encounter. The minor radius at time $t$ after the encounter is given by $r_m = r_{m_0}(1 + t/T_0)$.

[b]Here $\theta_n$ and $\phi_n$ are the latitude and longitude angles of a vector normal to the torus plane defined by the axial magnetic field. The function $sgn(B_x)$ is the sign of the $B_x$ component of the axial field, indicating on which side of the torus the spacecraft encountered.

[c]Here $(p_y, p_z)$ indicates the position of the spacecraft track from the torus axis in the $Y$-$Z$ plane; $p$ is the minimum distance from the torus axis to the spacecraft; all in the unit of $r_{m_0}$.

[d]$B_T$ is a parameter to determine the intensity of the toroidal magnetic field [see *Marubashi and Lepping*, 2007].

[e]$U_{T_0}$ is the bulk velocity of MC at the time of encounter, and the velocity changes afterward as $U_T(t) = U_{T_0} - D_f t$.

[f]$H$ is the handedness of the twist (R for right handed and L for left handed).

[g]$T_0$ is a time constant describing a self-similar expansion (see footnote a).

[h]$E_{rms}$ is the error-estimating figure defined by equation (1) in the text.

generally agree, though some cases are reported in which the helicity signs seem to disagree [*Leamon et al.*, 2004]. The helicity sign of the MC of 20 November 2003 was found to be positive (right handed) in all of the above-cited studies. On the other hand, it is not always simple to determine the helicity sign of the solar active region from observations. In fact, *Chandra et al.* [2010] pointed out many morphological features indicating that AR 10501 had a global negative helicity as a whole. However, these authors succeeded to show the existence of a region of positive helicity localized in the southern part of AR 10501, by more detailed fitting applied separately to specific groups of observed field lines. Thus, they could finally identify the precise source region from which the MC of 20 November erupted.

[4] Many foregoing studies suggested that the orientations of MC axes are commonly nearly parallel (within $\pm30°$) to the orientations of the magnetic inversion lines of their associated solar sources [*Marubashi*, 1997; *Bothmer and Schwenn*, 1998; *Yurchyshyn et al.*, 2001; *Marubashi et al.*, 2009]. It should be noted here, however, that recent studies pointed out the possibility of CME rotation both in the lower corona and in interplanetary space [*Yurchyshyn et al.*, 2009; *Shiota et al.*, 2010; *Vourlidas et al.*, 2011]. The axis orientation of the 20 November 2003 MC was estimated in previous studies with 2-D models with all conditions being constant along a straight axis. Their results generally agree on the orientation at 1 AU being largely tilted southward, with the tilting angles ranging from $-49°$ to $-87°$. When the estimated orientation of the MC axis was compared with the solar observations, difficulties arose because of the U-shaped inversion line as indicated by the U-shaped filament. As a result, several different ideas were proposed for the original orientation, which the MC might have had near the time of eruption from the corona. They include the following suggestions: (1) that the orientation may have been

affected by the nearby coronal hole [*Gopalswamy et al.*, 2005], (2) that the original MC orientation might be parallel to a line connecting two foot points of the erupted filament [*Yurchyshyn et al.*, 2005], and (3) that the MC orientation may take any direction parallel to tangent at some point of the U-shaped inversion line [*Wang et al.*, 2006]. Among others, the source region identified by *Möstl et al.* [2008] coincides with the source region identified later by *Chandra et al.* [2010]. Because the original orientation is different from the MC axis near the Earth by about 90°, they invoke a possible rotation of the axis during propagation through interplanetary space so as to be more aligned to the heliospheric current sheet (HCS) as suggested by *Mulligan et al.* [1998].

[5] Thus, the determination of MC axis orientation is an important key to understanding the link of interplanetary MC to the associated solar eruption event. So far, the axis orientation of the 20 November 2003 MC was estimated by using MC models that assume a 2-D structure. If we take the global MC structure to be a loop of magnetic flux rope extending from the Sun as commonly accepted, cylindrical models are applicable only to those cases where the spacecraft passed through the MC near the apex of the loop. For the spacecraft encounter with the curved portion of the MC near the flank of the loop, curvature of the MC must be taken into account to explain the observed magnetic field variations [*Marubashi*, 1997; *Marubashi et al.*, 2009]. The 20 November 2003 MC provides one challenging example to test this idea. The aim of this study is to find out possible geometries of this particular MC that fit the observed solar wind variations by applying the torus model [*Marubashi and Lepping*, 2007] and to see what physical picture emerges about the connection between the MC and the associated solar event.

[6] We start with the analyses of the 20 November 2003 MC with both torus and cylinder models in section 2. We then compare the result from each analysis with other solar

**Table 2.** MC Parameters Determined by Cylinder Fitting

| Model ID[a] | Start Day and Time (UT) | End Day and Time (UT) | $r_0$[b] (AU) | $\theta_a$[c] (deg) | $\phi_a$[c] (deg) | $p$[d] ($r_0$) | $U_0$[e] (km s$^{-1}$) | $B_0$[f] (nT) | $T_0$[g] (h) | $H$[h] | $E_{rms}$[i] |
|---|---|---|---|---|---|---|---|---|---|---|---|
| | | | | | *Present Results* | | | | | | |
| E | 20 Nov 2003 11:00 | 21 Nov 2003 00:30 | 0.073 | −66.2 | 137.3 | 0.23 | 598 | 72.7 | 23 | R | 0.174 |
| F | 20 Nov 2003 11:00 | 20 Nov 2003 19:20 | 0.053 | −42.8 | 135.9 | 0.42 | 610 | 69.6 | 58 | R | 0.151 |
| E′ | 20 Nov 2003 12:00 | 21 Nov 2003 02:00 | 0.077 | −67.7 | 122.6 | 0.13 | 606 | 63.6 | 23 | R | 0.165 |
| F′ | 20 Nov 2003 12:10 | 20 Nov 2003 20:50 | 0.058 | −51.1 | 58.5 | −0.24 | 622 | 59.1 | 50 | R | 0.160 |
| | | | | | *Previous Results* | | | | | | |
| Ly | 20 Nov 2003 10:00 | 21 Nov 2003 02:00 | 0.105 | −86.8 | 172.1 | 0.00 | 584 | 42.9 | – | R | – |
| Yu | 20 Nov 2003 10:11 | 20 Nov 2003 19:43 | – | −46.8 | 112.2 | – | – | – | – | R | – |
| Wa | 20 Nov 2003 10:06 | 21 Nov 2003 00:24 | – | −55 | 90 | 0.00 | – | 50.0 | – | R | – |
| Mö | 20 Nov 2003 11:16 | 20 Nov 2003 18:44 | – | −55 | 80 | ∼0 | 615 | – | – | R | – |
| Lp | 20 Nov 2003 10:48 | 21 Nov 2003 02:18 | 0.067 | −76 | 217 | 0.03 | 599 | 38.3 | – | R | 0.175 |

[a]The model IDs are as follows. E, the longer interval ACE data; F, the shorter interval ACE data; E′, the longer interval Wind data; F′, the shorter interval Wind data; Ly, *Lynch et al.* [2005]; Yu, *Yurchyshyn et al.* [2005]; Wa, *Wang et al.* [2006]; Mö, *Möstl et al.* [2008]; Lp, *Lepping et al.* [2006].
[b]Here $r_0$ is the cylinder radius at the time of encounter. The radius at time $t$ after encounter is given by $r(t) = r_0(1 + t/T_0)$.
[c]Here $\theta_a$ and $\phi_a$ are the latitude and longitude angles of the cylinder axis field.
[d]Here $p$ is the impact parameter in the unit of $r_0$.
[e]$U_0$ is the bulk speed of the MC cylinder.
[f]$B_0$ is the magnetic field intensity at the cylinder axis.
[g]$T_0$ is a time constant describing a self-similar expansion (see footnote a).
[h]$H$ indicates the handedness of the twisting field (R for right handed and L for left handed).
[i]$E_{rms}$ is the error-estimating figure defined by equation (1) in the text.

and interplanetary observations and attempt to determine which model provides more reasonable explanation in section 3. Our conclusions are given in section 4.

## 2. Analysis of Solar Wind Data

### 2.1. Naming of Fitting Cases

[7] In this section, we attempt to find out all possible geometries of flux ropes that can explain the observed magnetic field variation in the MC. For this purpose, we apply the least squares–fitting method with two different flux rope models, a cylinder model and a torus model. We need to select the start and end times of the MC from the time variation of the solar wind data, and it is not always easy to point the start and end times. Therefore, we tried two possible intervals for our fitting analysis, which we call a longer duration and a shorter duration, respectively.

[8] As a result of the analysis, we found three possible geometries, two torus geometries and one cylinder geometry, for each of the selected durations. We also performed the same analysis for data from ACE and data from Wind. Here we summarize the cases of fitting and the corresponding naming. Two torus geometries for the longer interval with ACE data are indicated by A and B in Table 1, and the corresponding cylinder case is designated as E in Table 2. For the shorter interval, two torus cases are C and D in Table 1, and the cylinder case is F in Table 2. We also obtained similar results from the Wind data, and they are correspondingly called A′, B′, and E′ for the longer interval and C′, D′, and F′ for the shorter interval, respectively.

[9] It is worthwhile to mention the accuracy of the parameter determination from the fitting. Although it is not easy to estimate the accuracy, we can safely say that changes of the axis direction of 10° do not cause for the calculated magnetic fields to change very much (typically <10%). This estimate should be taken as a rough one based on the experimental calculations for several cases.

### 2.2. Fitting With a Torus Model

[10] Figure 1 shows the solar wind observations from ACE for 2 days, 20–21 November 2003, together with the results of torus-model fittings for the two possible selected MC boundaries. Plotted are from the top, the magnetic field intensity ($B$), the $X$, $Y$, and $Z$ components of the field in the GSE coordinate ($B_x$, $B_y$, $B_z$), the ratio of standard deviations to the average intensities ($Sb/B$), the proton bulk speed ($V_{sw}$), the proton number density ($N$), the number density ratio of He$^{++}$/H$^+$, the proton temperature ($T$), and the plasma beta based on protons, all from 64 s averages. A shock detected at 07:27 UT, 20 November, is indicated by the vertical dashed line. The second panel is the plot of pitch angle distribution of electrons in the 272 eV channel, showing 5 min averages normalized to the maximum flux value in each time bin. The third panel presents vector plots of 30 min averages of magnetic field projected on the $X$-$Y$, $X$-$Z$, and $Y$-$Z$ planes. The dashed curve drawn along the proton temperature shows the temperature statistically expected from the proton bulk speed, $T_{ex}$ [*Lopez*, 1987] calculated with 30 min averages. The low values of the $T_{ex}/T$ ratio are commonly used as an indicator of interplanetary coronal mass ejections (ICME) [*Cane and Richardson*, 2003].

[11] We selected the start time of the MC at 11:00 UT, 20 November (black solid line), and two possible end times at (1) 00:30 UT, 21 November (red line), and (2) 19:20 UT, 20 November (blue line). The selection of the MC interval is based on the following characteristics: the smooth magnetic field rotation mainly in the $Y$-$Z$ plane, the relatively small fluctuation level ($Sb/B$), the relatively low values of $T_{ex}/T$, the low beta values, and the bidirectional flow of superthermal electrons. The shorter interval was taken to be a possible limit of the MC because the magnetic field rotation becomes weak at 19:20 UT, although other plasma and magnetic field characteristics suggest that the MC interval continues till 00:30 UT, 21 November.
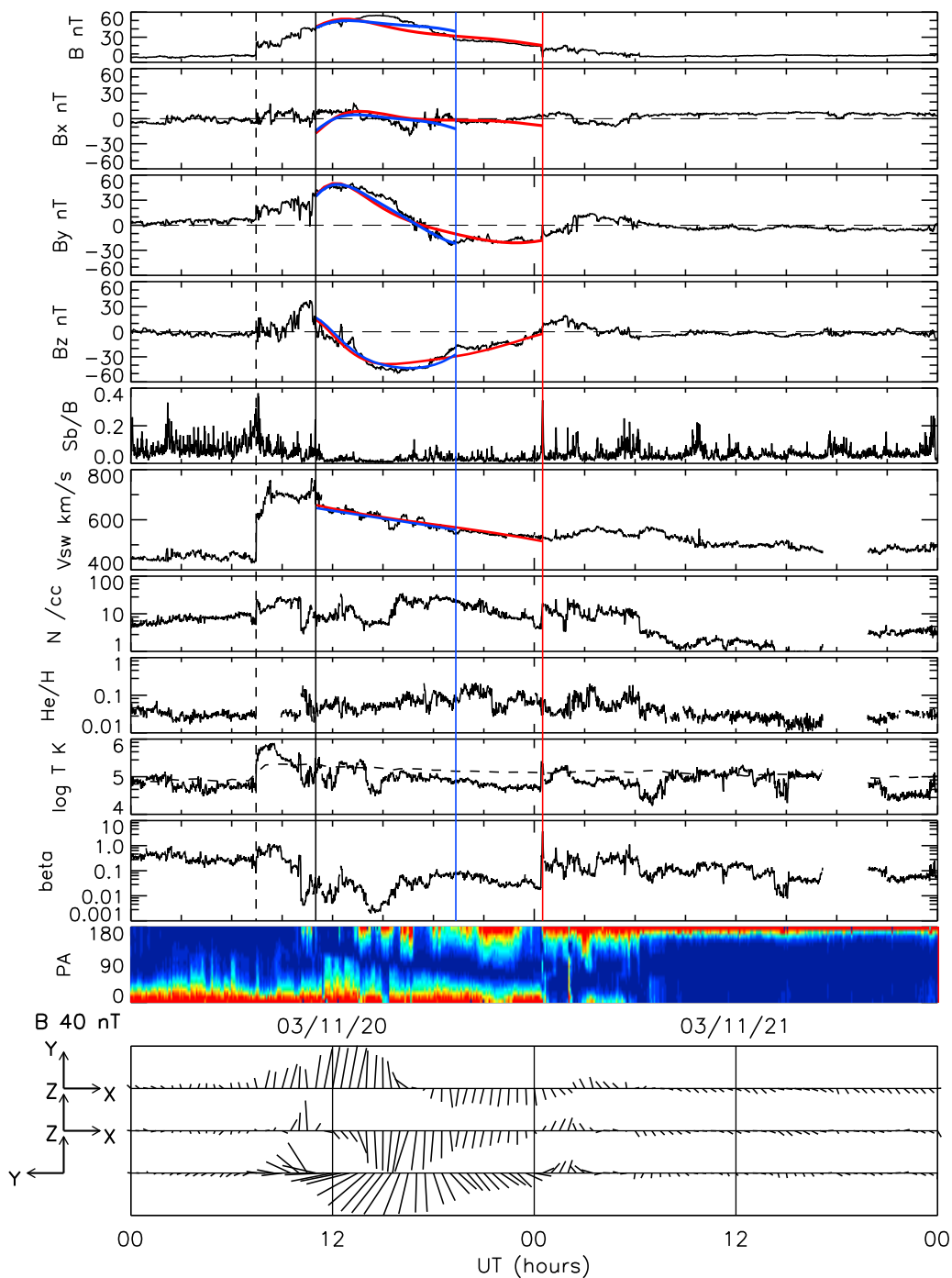
**Figure 1.** Results of the torus fitting for the two possible MC intervals superimposed on the data plots of the observed solar wind parameters. The red line is for the longer interval (case A in Table 1, 20 November 11:00 UT to 21 November 00:30 UT), the blue line for the shorter interval (case C in Table 1, 20 November 11:00 UT to 19:20 UT). The vertical dashed line indicates the time of shock arrival. The magnetic field vectors projected on the *X-Y*, *X-Z*, and *Y-Z* planes is shown at the bottom.

[12] The results of fitting with a torus model [*Marubashi and Lepping*, 2007; *Romashets and Vandas*, 2003] are presented by the red curve for the longer interval (case A) and by the blue line for the shorter interval (case C). It is seen that the fitting reproduces the observation pretty well for both interval selections. The parameters obtained from the fitting are summarized in Table 1, together with those from other fittings (as summarized in section 2.1). The accuracy of fitting can be estimated by

$$E_{\mathrm{rms}} = \sqrt{\sum_i \left( \bar{B}_i^O - \bar{B}_i^M \right)^2 / N} / \bar{B}_{\max}^O. \qquad (1)$$
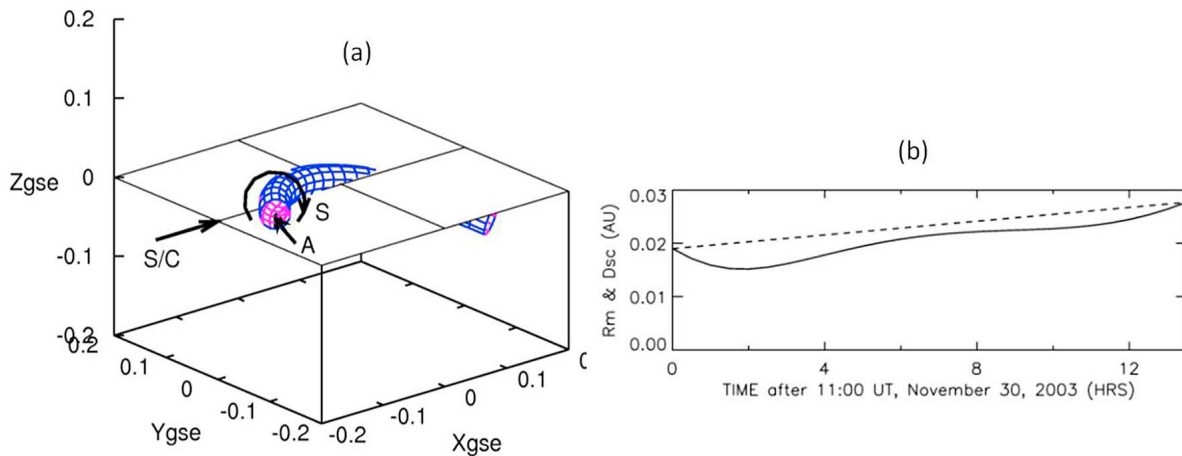
**Figure 2.** The geometry of the spacecraft encounter with the MC determined for case A: (a) a 3-D presentation and (b) the time variation of the minor radius of the toroidal MC (dashed line) and the variation of distance from the axis to the spacecraft (solid line).

Here $\bar{B}_i^O$ and $\bar{B}_i^M$ are the $i$th magnetic field vectors from observation and model ($i = 1, ..., N$), respectively, and $\bar{B}_{max}^O$ is the maximum value of the observed field intensity in the MC interval. The $E_{rms}$ values are 0.215 for the longer interval and 0.213 for the shorter interval.

[13] Figure 2 depicts the geometry of the MC encounter with the spacecraft for the case of longer interval. Figure 2a is a 3-D presentation, in which three arrows indicate the spacecraft path relative to the curved structure (arrow annotated S/C), the direction of magnetic field on the MC surface (arrow S), and the direction of magnetic field on the MC axis (arrow A). It is seen that the main body of the MC passed the westside relative to the Sun-Earth line and that only its eastern flank swept the Earth. The greatest contribution to the southward magnetic field of this particular MC comes from the toroidal (perpendicular to the axis) field component near its inside surface. In Figure 2b, the dashed line shows the time variation of the radius (minor radius of torus, $r_m$) of the modeled MC, which increases due to expansion assumed in our model, based on the theoretical work by *Farrugia et al.* [1993] and later modification by *Shimazu and Vandas* [2002]. The solid line shows the time variation of distance from the axis to the spacecraft ($D_{sc}$). It should be noted that the spacecraft stayed for a long time near the inner side surface of the structure, particularly in the later part of the MC, where the magnetic field does not change greatly. The expansion of the torus contributes much to the long-time stay of the spacecraft within the cloud. A similar result is obtained for the encounter geometry for the MC fitting with the shorter interval, although the tilt angle of the torus plane is slightly different. (No figure is shown. Details are presented in Table 1.)

[14] In the original idea of self-similar expansion [*Farrugia et al.*, 1993], the expansion parameter $T_0$ physically corresponds to the time spent by the MC from the generation to the encounter with the spacecraft. In this sense, the value for case A ($T_0 = 30$ hours) looks unrealistically small, but this value is well within the range of $T_0$ obtained for many other cases. It can be said in this particular case that the small $T_0$ value is attributable to the compression of

the MC on the frontside. Such asymmetry in magnetic field intensity causes to yield small $T_0$ in our fitting routine.

[15] If we assume that the global MC loop is contained nearly in a plane, the tilt angle of the plane (particularly near the apex of the MC loop) can be estimated using the direction of a normal vector to the torus plane obtained from the fitting. Figure 3a depicts the projection on the $Y$-$Z$ plane of the whole torus determined by the fitting for the longer interval. (We are not arguing that the actual MC has a torus shape. The torus is just a local approximation of the MC at the portion where the spacecraft traversed the structure.) In Figure 3a, the red dot indicates where the spacecraft encounters the MC, and the two red arrows indicate the directions of magnetic field along the axis and the surface field. The normal vector is defined by the circle depicted by the axis field. The local direction of the axis field at the apex (farthest point from the Sun) projected on the $Y$-$Z$ plane is calculated as follows:

$$\Phi = \tan^{-1}\left(\frac{\cos\theta_n \cdot \sin\phi_n}{-\sin\theta_n}\right), \qquad (2)$$

where $\Phi$ is the angle measured clockwise in this presentation from $y$ axis, and $\theta_n$ and $\phi_n$ are latitude and longitude angles of the normal vector, respectively (from 0° to 360° depending on the sign of $\cos\theta_n \cdot \sin\phi_n$ and $-\sin\phi_n$). This direction can be taken as an approximate estimate of the MC direction expected near the solar source when the observed MC is traced back to the Sun with its direction maintained. The corresponding flux rope cylinder is also depicted in Figure 3a. The $\Phi$ values are 11.1° and 30.3° for the longer and shorter intervals, respectively. These values are close to the direction of the post-eruption arcade (PEA) formed in AR 10501 after the source event, as will be discussed later.

[16] One noteworthy feature of the spacecraft encounter with the MC discussed above is that the spacecraft does not penetrate deeply into the MC (see Figure 2b). In such cases, the torus fitting sometimes returns another possible result. In an effort to search for other possible geometries that can explain the observation, we found another good fit, which is shown in Figure 4. In Figure 4, only the magnetic fields and
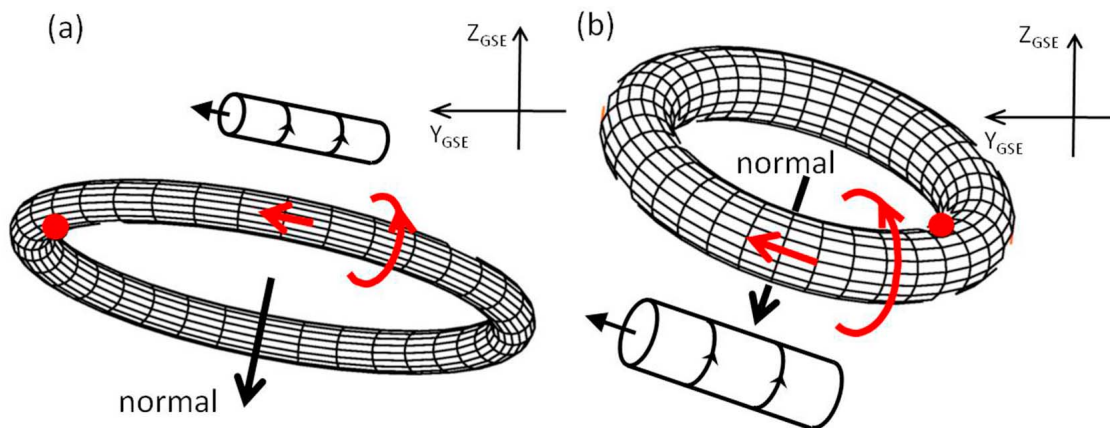
**Figure 3.** The projection on the *Y-Z* plane of the whole torus corresponding to the two possible geometries determined by the fitting for the longer interval: (a) case A in Table 1 and (b) case B in Table 1. In Figures 3a and 3b, the red dot indicates the spacecraft pass (perpendicular to Figure 3), and the directions of magnetic field along the axis and the surface field are indicated by two red arrows. Note that the spacecraft passes through the torus flank with a positive axial field in case A and through the torus flank with a negative axial field in case B. The approximate MC orientation at the torus apex is schematically indicated by a cylinder.

the proton speeds are plotted because other parts are the same as Figure 1. Again, the red and blue curves present the fitting results for the two intervals selected as the MC. The $E_{rms}$ values are 0.165 for the longer interval and 0.143 for the shorter interval, the fitting accuracy being better in these fittings.

[17] Figure 3b depicts the torus geometry that was obtained for the longer interval in the same way as Figure 3a.

This result indicates that the main body of the MC passed the eastside of the Sun-Earth line and that the western flank encountered the Earth. The torus tilt angle in this case is such that the frontside is on the southside compared with the rear side, being opposite to the case of Figure 3a. However, the magnetic field direction at the apex is similar to that in Figure 3a as indicated by the schematic cylinder flux rope approximating the structure near the apex. Here we note
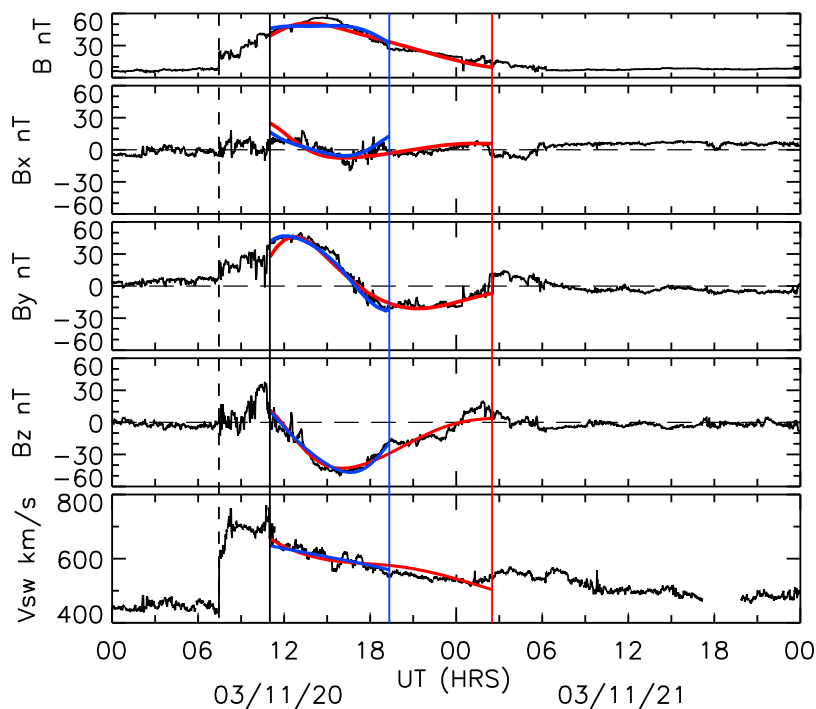


**Figure 4.** Results of the torus fitting for the two possible MC intervals superposed on the plots of the observed magnetic field variations. Note that the parameter sets obtained from the fitting are different from those depicted in Figure 1. The red line is for the longer interval (case B in Table 1), and the blue line is for the shorter interval (case D in Table 1).
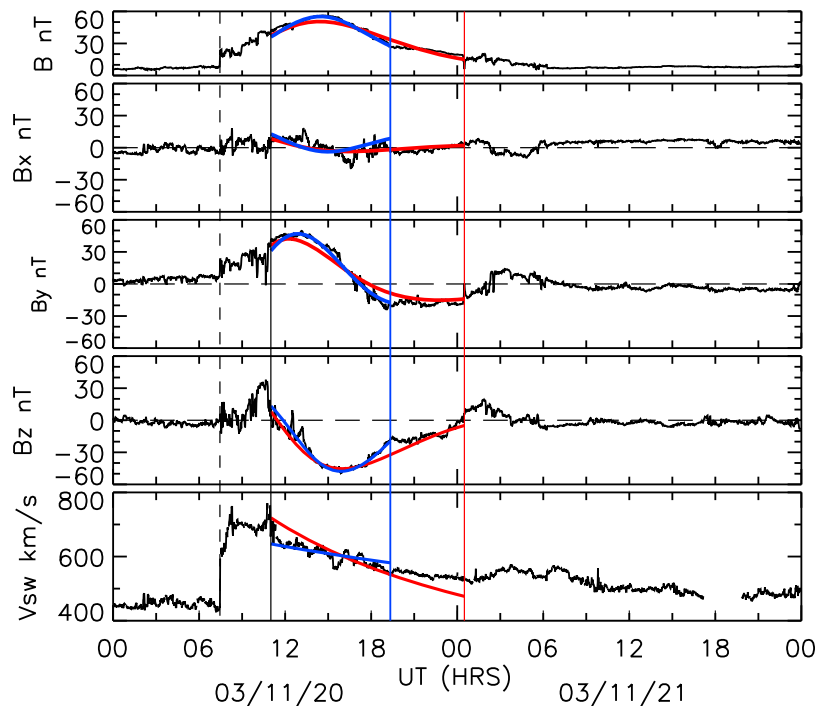
**Figure 5.** Results of the cylinder fitting for the two possible MC intervals superposed on the lots of the observed magnetic field variations. The red line corresponds to the parameter sets of case E in Table 2, and the blue line corresponds to case F in Table 2.

another important difference between these two geometries of spacecraft encounter. In the case of Figure 3a, the spacecraft passed through the structure, where the axial field has a positive $X$ component, whereas the $X$ component of the axial field is negative in the case of Figure 3b. This difference is denoted by $Sgn(B_x)$ in Table 1.

[18] In order to find out which fitting provides the most appropriate geometry of the actual MC, we need to compare the fitting results with other solar and interplanetary observations, which is the subject of the next section. We also mention the possibility that a comparison of MC data from two spacecraft might give us a clue for the selection of the most realistic geometry. With this idea in mind, we performed the same analysis with the solar wind data from Wind. Unfortunately, the distance between ACE and Wind in the $Y$-$Z$ plane is too small compared with the scale of the MC. The average positions of the two spacecrafts are (240, 26, and −9) $R_E$ for ACE and (−212, −38, and −13) $R_E$ in GSE. The separation in the $Y$-$Z$ plane is about 64 $R_E$ in the east-west direction, whereas the minor radius of the torus MC is in the range of 0.014–0.034 AU (330–800 $R_E$). Thus, the fitting results from the ACE and Wind spacecraft are very similar. The parameters obtained by the torus fitting for all the cases for both spacecraft are summarized in Table 1. It should be noted here that the difference between two torus planes is expressed by the angle between two vectors normal to two torus planes. The difference in the axis' direction between models A and A′ is 9.8° and 9.5° between B and B′.

### 2.3. Fitting With a Cylinder Model

[19] We also tried the fitting with a cylinder model [*Marubashi and Lepping*, 2007], and the results are shown in Figure 5 for the two intervals: the longer interval in red

and the shorter interval in blue. We can see that the cylinder fitting yields a good fit to the observation as does the torus fitting. The parameters determined by the fitting are presented in Table 2, together with the results obtained from the corresponding Wind data. We notice that the results for ACE and Wind for the longer MC interval roughly coincide with each other, whereas those for the shorter interval show a significant difference in the MC axis direction. It should be also noted here that the cylinder radius values are generally much larger (by a factor of ∼3) compared with the values of torus minor radius. The reason for this difference is that the spacecraft traverses through the MC structure more in parallel to the axis in the case of the MC flank passage.

[20] There exist several model fitting results with 2-D models with physical quantities being constant along the straight axis for this MC as mentioned in section 1. Table 2 includes the MC axis directions and impact parameters published in the literature for the purpose of mutual comparison. For other parameters, the direct comparison is not appropriate because of the differences in the models and the data that are used. Listed are the fitting with a cylindrical model of force-free flux rope applied to the ACE data [*Lynch et al.*, 2005; *Wang et al.*, 2006], fitting with a same model but applied to the Wind data [*Lepping et al.*, 2006], fitting with a cylindrical model allowing a self-similar expansion (present analysis); the Grad-Shafranov (GS) reconstruction applied to the ACE data [*Yurchyshyn et al.*, 2005], and the GS reconstruction applied to the ACE and Wind data simultaneously [*Möstl et al.*, 2008]. Two different MC boundaries were selected in the previous studies, roughly, similar to our selection of two possible MC intervals. The results generally indicate that the MC axis is highly inclined southward from the ecliptic plane, though the
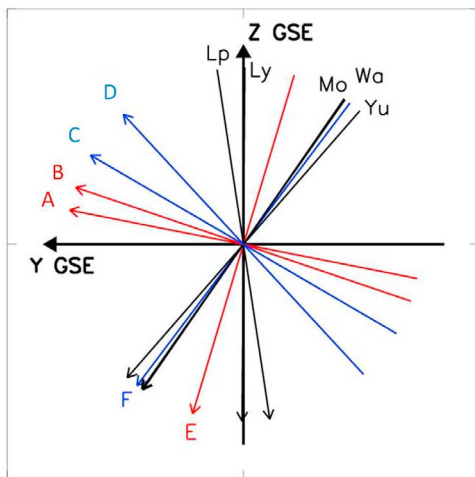
**Figure 6.** Comparison of the MC axis directions projected onto the *Y-Z* plane determined with different cylinder models (Lp, *Lepping et al.* [2006]; Ly, *Lynch et al.* [2005]; Mo, *Möstl et al.* [2008]; Wa, *Wang et al.* [2006]; Yu, *Yurchyshyn et al.* [2005]). Vectors E and F present results for long and short intervals, respectively. Vectors A and B represent the projected directions of the cylinders approximating the torus MC at the apex (depicted in Figure 3), and vectors C and D show the corresponding directions obtained for the shorter MC interval.

resultant inclinations are smaller for the shorter chosen MC intervals as noted by *Möstl et al.* [2008]. The impact parameter for the shorter interval obtained in this study ($p = 0.42$) is significantly larger than the others, but this is consistent with the observation that the rotation angle of the magnetic field vector is appreciably smaller than 180°. It is rather surprising that the direction of the MC axis obtained from the fitting changes so much depending on the model.

[21] It is worthwhile to note one character of our model in contrast with other models mentioned above. In our fitting routine, the expansion of MC is taken into consideration based on a self-similar expansion model [*Farrugia et al.*, 1993]. The expansion affects the time variations of observed magnetic field and solar wind speed within the MC. The dynamic effects are described by one parameter $T_0$ (see *Marubashi and Lepping* [2007] for details). In other words, the asymmetry of magnetic field and the change in solar wind speed are considered simultaneously. In contrast, all foregoing studies are based on the model in which the MC structure is assumed to be unchanged.

[22] In order to compare the MC direction with the magnetic field structure in the solar source region, we calculated the MC axis direction projected onto the *Y-Z* plane using the equation:

$$\Phi_a = \tan^{-1}\left(\frac{\sin\theta_a}{\cos\theta_a \cdot \sin\phi_a}\right), \qquad (3)$$

where $\Phi_a$ is measured from $y$ axis, ranging from 0° to 360° depending on the signs of $\sin\theta_a$ and $\cos\theta_a \cdot \sin\phi_a$. This angle represents the direction of the flux rope structure near the Sun at the time of eruption, if we assume that such a flux rope propagates through interplanetary space with its axis

maintained and if the modeled cylinder is taken as an approximation of the MC loop near its apex. In Figure 6, we compare $\Phi_a$ values calculated from the axis parameters in Table 2 and the corresponding $\Phi$ values from the torus parameters (equation (2)). Here we emphasize again that the 2-D model and the torus model yield a big difference in the estimated direction of the flux rope created near the Sun, roughly being 90° for this particular MC.

[23] Finally, we calculate the normal vector of the shock at 07:27 UT preceding the MC, because it is expected that the direction of shock normal provides constraint about the geometry of a shock driver. We used the expression given by *Berdichevsky et al.* [2000] and obtained the following results: $n = (-0.925, 0.311,$ and $-0.218)$ in GSE coordinates or in longitudinal and latitudinal angles, $\phi_s$ and $\theta_s$, $\phi_s = 161.4°$ and $\theta_s = -12.6°$. The shock normal is directed about 20° eastward from the Sun-Earth line, and about 10° southward from the ecliptic plane, suggesting that the MC geometry in Figure 3a is more consistent with that in Figure 3b.

## 3. Comparison With Solar and 2-D Heliospheric Observations

[24] It has been shown thus far that three different MC geometries can reproduce the observed magnetic field variations with satisfactory accuracy for each of the MC interval selection: two torus geometries and one cylinder geometry. *Möstl et al.* [2008] took the later part of the longer interval (19:20 (20 November) to 00:30 UT (21 November)) as the region that remained on the rear side of the main body of the MC with the field lines on the leading side being peeled off as a consequence of the reconnection with the solar wind ahead of the MC [*Dasso et al.*, 2006]. As has been shown, the torus model properly describes the field observations at the rear side of the MC, and the couterstreaming electrons continued to be observed long after 19:20 UT, 20 November (Figure 1). Therefore, we take the longer interval as the proper MC interval. In this section, we attempt to determine which geometry provides the most coherent interpretation of the observed MC by comparing with other solar and interplanetary observations.

[25] We first consider the solar events that can be taken as the origin of the MC. AR 10501 produced two successive M-class flares on 18 November 2003 at N00E18, both being followed by CMEs: M3.2/2N flare at 07:52 UT (maximum) followed by a CME having first appeared in the LASCO C2 field of view at 08:06 UT and M3.9/2N flare at 08:30 followed by another CME detected first at 08:50 UT. Hereinafter, these two CMEs are called CME 1 and CME 2, respectively, in accordance with *Gopalswamy et al.* [2005], and the corresponding flares as flare 1 and flare 2. CME 2 is a halo CME having an initial speed of about 1660 km/s, whereas CME 1 was estimated to have an angular width of 104° and the initial speed of about 1220 km/s. The metric type II bursts were reported, with intensity index 3 for flare 1 and index 2 for flare 2 (event list from NOAA/Space Weather Center in http://www.solarmonitor.org/). Both events are well within a reasonable time window as a source event for the 20 November 2003 MC. The transit time of the MC from the Sun to the Earth is estimated to be 63 hours if we assume a constant speed of 650 km/s (Table 1). The actual time lag from the flare to the MC start time is about 8 hours shorter,
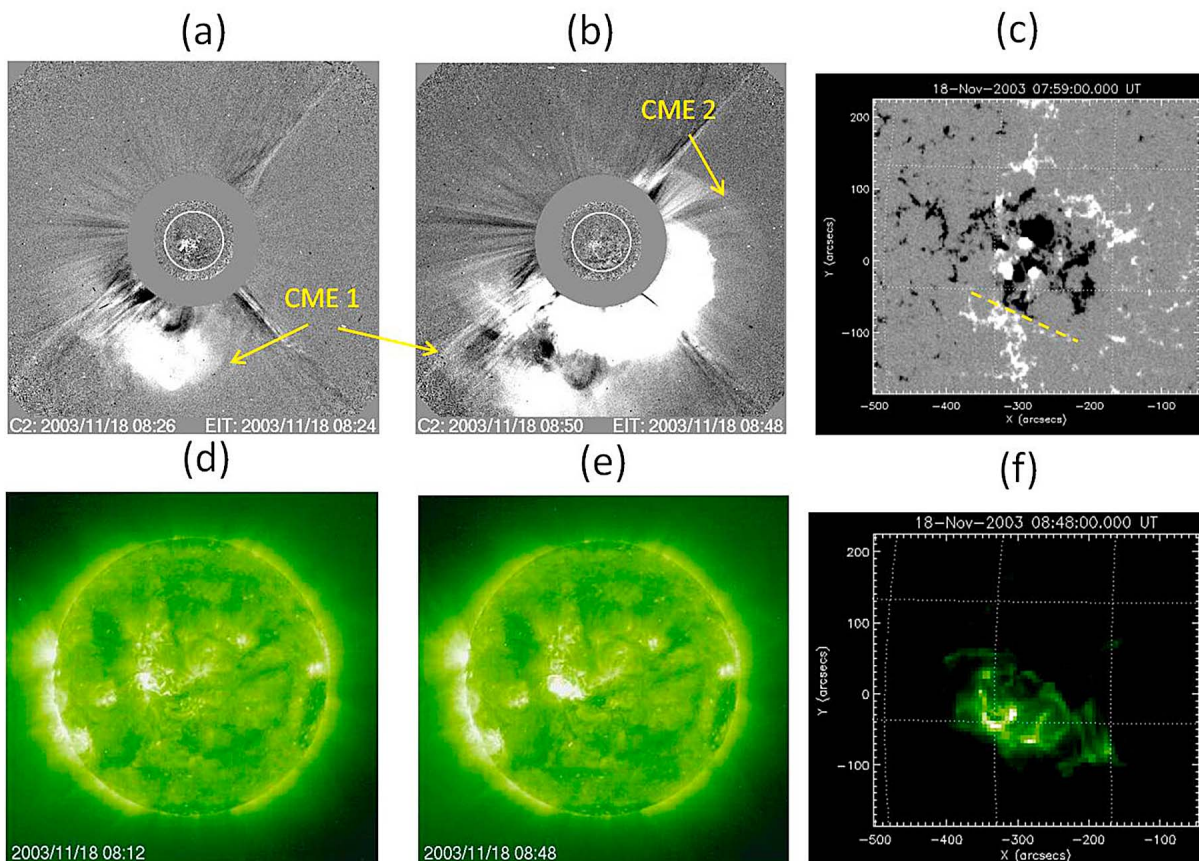
**Figure 7.** Images of CMEs, associated activities in the solar atmosphere, and the magnetic field structure in their source region on 18 November 2003: (a) the LASCO C2 difference image at 08:26 UT, (b) the same but at 08:50 UT, (c) the MDI image of AR 10501 at 07:59 UT with the polarity inversion line indicated by the yellow dashed line, (d) the EIT 195 image at 08:12 UT, (e) the same but at 08:48 UT, and (f) the partial image of EIT 195 at 08:48 with enhanced contrast for the PEA.

indicating deceleration during the propagation. There was no other prominent eruption event that may be taken as a possible origin of the MC in the time window of ±24 hours around these two events.

[26] Figure 7 presents the selected image data that are relevant to the activities responsible to the formation of the 20 November 2003 MC. Figures 7a and 7b are images of CME 1 and CME 2 from SOHO/LASCO C2 coronagraph with Figure 7a at 08:26 UT, showing the most extending state of CME 1 before CME 2 appears in the field of view, and Figure 7b at 08:50 UT, the first appearance of CME 2. Figures 7d and 7e are the SOHO/extreme ultraviolet imaging telescope (EIT) 195 observations Figure 7d at 08:12 UT, the last time before flare 2, giving an indicator of the possible formation of the PEA although not clear because the early stage of two ribbons of flare 2 already present, and Figure 7e at 08:48 UT showing the well-developed PEA of flare 2. The LASCO and EIT images were taken from SOHO LASCO CME CATALOG (http://cdaw.gsfc.nasa.gov/CME_list). Figure 7c shows the distribution of longitudinal magnetic fields in AR 10501 from the SOHO/Michelson Doppler Imager (MDI) observation, where the approximate position of the polarity inversion line is indicated by the yellow dashed line. Figure 7f presents the partial image of EIT 195 at 08:48 UT with the contrast being enhanced for the PEA to be

clearly seen. (For EUV solar images, Transition Region and Coronal Explorer (TRACE) 171 observations provide images with much higher resolution, and some images from TRACE are used in the discussion of the eruption by *Möstl et al.* [2008]. However, there is no TRACE 171 image available for the times just after flare 1 and flare 2. Therefore, we used SOHO/EIT images for the purpose to see the orientation of the PEA.)

[27] It is commonly accepted in the previous studies [*Gopalswamy et al.*, 2005; *Yurchyshyn et al.*, 2005; *Wang et al.*, 2006; *Möstl et al.*, 2008; *Chandra et al.*, 2010; *Schmieder et al.*, 2011] that the 20 November MC was produced in association with CME 2 because it is an energetic halo CME. We can see that the orientation of PEA axis (Figure 7f) is nearly parallel (∼30° to the north from $y$ axis) to the estimated initial direction of the flux rope produced in the corona (the cylinder in Figure 3a and arrow A in Figure 6, hereinafter we call the structure in Figure 3a as model A). The direction of $y$ axis in GSE coordinates tilted less than 2.5° southward from the solar equator in this period. The magnetic field polarity of the right-handed flux rope near the apex of the MC loop is also consistent with the magnetic field polarity of the PEA determined by *Chandra et al.* [2010]. Thus, the most straightforward interpretation about the link between the solar event and the MC is that a flux rope
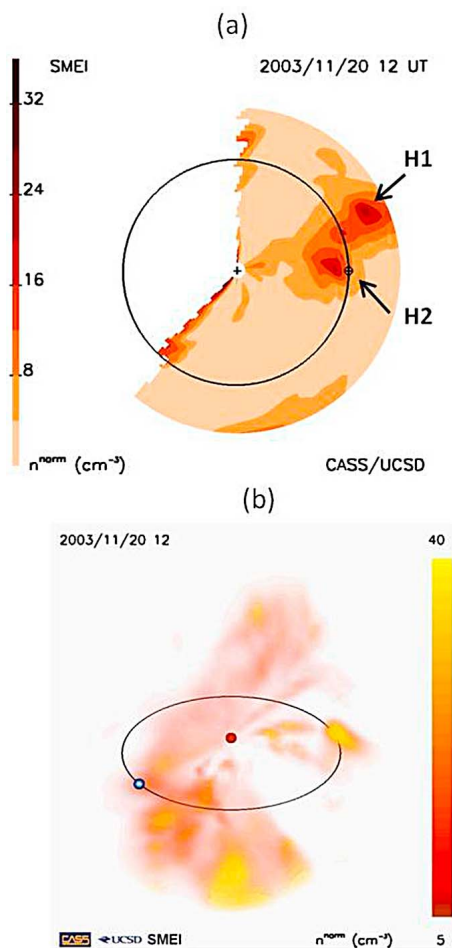
**Figure 8.** (a) The ecliptic cut and (b) the 3-D view of density distribution in interplanetary space at 12:00 UT, 20 November 2003, obtained from the SMEI 3-D reconstruction (courtesy of B. Jackson).

produced as a main body of CME 2 propagated through interplanetary space a little westward from radial direction with its orientation maintained and that the eastern flank was traversed by ACE. This scenario is consistent with the observational fact that CME 2 was initially launched westward. The shock normal directed about 20° eastward also supports the interpretation that the observed MC is the eastern flank of model A. We expect that the global configuration of the MC should be a loop of magnetic flux rope with both legs rooted near the both ends of PEA and extending toward interplanetary space. This expectation is strongly connected to the suggestion that the signature of PEA is taken to be CME proxy just after the initial launch [*Tripathi et al.*, 2004]. The observed signatures of the MC are strongly controlled by what part of the loop was traversed by the spacecraft.

[28] We now examine the data obtained from the Solar Mass Ejection Imager (SMEI) [*Jackson et al.*, 2004]. Figure 8a shows the ecliptic cut and Figure 8b shows the 3-D view at 12:00 UT, 20 November, obtained by the SMEI 3-D reconstructions (by the courtesy of B. Jackson). We can see a high-density region passing the Earth orbit, which extends westward from the Earth position. A similar density distribution was also obtained from Ooty radio telescope scintillation

observations [*Schmieder et al.*, 2011]. If this high-density region is taken to be representing the ICME, the SMEI observation supports the association of the MC model A and CME 2. Fortunately, this comparison is possible because this MC coincides with the high-density region.

[29] However, closer examination of SMEI reconstruction images suggests another possibility though less plausible than the above suggested link. The high-density region consists of two substructures, labeled H1 and H2 in Figure 8. The earlier images show that the substructure H1 passed 1 AU on the westside of the Earth without encounter. It is thus not unreasonable to suppose that they are essentially separate structures, the substructure H2 corresponding to the western flank of the MC model B. Then, CME 1 can be taken as the source event of the MC. This view is consistent with the fact that CME 1 was initially launched eastward. The launching site of CME 1 is a little more eastward from that of CME 2, where the polarity inversion line is tilting a little more than that of source region of CME 2. This may be consistent with the difference in the estimated direction of the flux rope created in the corona (arrows A and B in Figure 6), although the difference is not significant compared with the accuracy of the fitting analysis. If we take this interpretation, the substructure H1 should be ascribed to the ICME associated with CME 1, which just did not encounter the Earth. It is highly plausible that both CME 1 and CME 2 produced MCs independently. This interpretation for the origin of the 20 November 2003 may not be likely, however, because the SMEI images do not show strong evidence for the existence of high-density region on the eastside of the Sun-Earth line. Another negative evidence is that the density distribution from interplanetary shock observations [*Schmieder et al.*, 2011] simply shows a single high-density region extending from around the Earth to the west. We must admit that the SMEI reconstruction maps may not have enough resolution to separate two high-density regions as shown in Figure 8a. However, it can be said that we cannot deny the possibility.

[30] Another outstanding phenomenon during the course of CME 1 and CME 2 is the eruption of filament around 08:00 UT from the apex of the U-shaped filament. Though the role played by this filament eruption in the sequence of activities is not clear, it is very unlikely that the CME 2 could be directly connected to the filament eruption. *Chandra et al.* [2010] clearly show that this segment of the filament has a dextral chirality and, therefore, left-handed magnetic helicity, which is opposite to the magnetic helicity of the 20 November MC.

[31] Finally, we discuss the fitting result with a cylinder model. It gives the axis direction nearly perpendicular to the magnetic polarity inversion line in the source region. In order to account for this discrepancy, *Möstl et al.* [2008] invoked possible rotation of the MC during propagation from the Sun to the Earth, so that the MC axis could be aligned along the HCS. They explain that this happened when the MC overtook the HCS and ran into the HCS. However, a close examination of Figure 1 shows the existence of a region of interplanetary magnetic field away from polarity during around 02:00 UT to around 06:00 UT, 21 November, just after the MC interval and a clear sector boundary from away to toward sector at around 06:00 UT. (We can see that $B_x$ and $B_y$ components changed sign simultaneously.) This sector boundary is more likely to be associated with the neutral line

in the source surface magnetic field provided by the Wilcox Solar Observatory (http://wso.stanford.edu/synsourcel.html). It is of course plausible that the MCs carry the newly formed HCSs as suggested by *Crooker et al.* [1998]. In such cases, the MC should be straddling the HCS (not global but local) with both feet on both sides of and near the solar magnetic neutral line.

## 4. Conclusions

[32] We have analyzed the MC of 20 November 2003 and compared with the available solar and interplanetary observations. The conclusions we obtained are summarized as follows.

### 4.1. Model Fitting Results

[33] 1. The observed magnetic field variations have been reproduced with satisfactory accuracies with three different geometries, two of which were determined by the torus model fitting and one was determined by the cylinder model fitting.

[34] 2. This result gives us an important caution that the least squares-fitting method cannot necessarily assure the uniqueness of the solution for the geometry of the MCs. It should be strongly recognized that the geometries obtained through model fittings are inevitably model dependent.

[35] 3. The estimated orientations of the global MC loop plane obtained from the torus model are found consistent with the direction of the PEA) formed in the solar source region in contrast to the result from the cylinder model.

### 4.2. Coherency With Other Observational Results

[36] 1. Two possible interpretations have been obtained about the link of the MC with the solar events. The common view in either interpretation is that a flux rope was produced in association with a CME nearly in parallel to the axis of the PEA and was propagated through interplanetary space with its axis direction maintained.

[37] 2. One scenario is that the observed MC was produced in association with the CME of 08:50 UT, 18 November 2003 (CME 2), and the eastern flank of the global MC loop encounter the Earth. This scenario implies that although an MC may have been produced by the CME of 08:06 UT, it passed the eastside of the Earth without encounter.

[38] 3. In the other scenario, the CME of 08:06 UT (CME 1) is the origin of the observed MC, though this scenario looks less likely than the first one. This interpretation implies that the ejecta possibly formed in association with the 08:50 UT CME passed the westside of the Earth without encounter.

[39] 4. In either of the two interpretations, the observed magnetic field variations in the MC are consistent with the field structure expected from the corresponding PEA structure.

## References

Berdichevsky, D. B., A. Szabo, R. P. Lepping, and A. F. Vinas (2000), Interplanetary fast shocks and associated drivers observed through the 23rd solar minimum by Wind over its first 2.5 years, *J. Geophys. Res.*, 105, 27,289–27,314, doi:10.1029/1999JA000367.

Bothmer, V., and R. Schwenn (1998), The structure and origin of magnetic clouds in the solar wind, *Ann. Geophys.*, 16, 1–24, doi:10.1007/s00585-997-0001-x.

Cane, H. V., and I. G. Richardson (2003), Interplanetary coronal mass ejections in the near-Earth solar wind during 1996–2002, *J. Geophys. Res.*, 108(A4), 1156, doi:10.1029/2002JA009817.

Chandra, R., E. Pariat, B. Schmieder, C. H. Mandrini, and W. Uddin (2010), How can a negative magnetic helicity active region generate a positive helicity magnetic cloud?, *Sol. Phys.*, 261, 127–148, doi:10.1007/s11207-009-9470-2.

Crooker, N. U., J. T. Gosling, and S. W. Kahler (1998), Magnetic clouds at sector boundaries, *J. Geophys. Res.*, 103, 301–306, doi:10.1029/97JA02774.

Dasso, S., C. H. Mandrini, P. Démoulin, and M. L. Luoni (2006), A new model-independent method to compute magnetic helicity in magnetic clouds, *Astron. Astrophys.*, 455, 349–359, doi:10.1051/0004-6361:20064806.

Démoulin, P. (2008), A review of the quantitative links between CMEs and magnetic clouds, *Ann. Geophys.*, 26, 3113–3125, doi:10.5194/angeo-26-3113-2008.

Farrugia, C., L. F. Burlaga, V. A. Osherovich, I. G. Richardson, M. P. Freeman, R. P. Lepping, and A. J. Lazarus (1993), A study of and expanding interplanetary magnetic cloud and its interaction with the Earth's magnetosphere: The interplanetary aspect, *J. Geophys. Res.*, 98, 7621–7632, doi:10.1029/92JA02349.

Gopalswamy, N., S. Yashiro, G. Michalek, H. Xie, R. P. Lepping, and R. A. Howard (2005), Solar source of the largest geomagnetic storm of cycle 23, *Geophys. Res. Lett.*, 32, L12S09, doi:10.1029/2004GL021639.

Jackson, B. V., et al. (2004), The Solar Mass Ejection Imager (SMEI) Mission, *Sol. Phys.*, 225, 177–207, doi:10.1007/s11207-004-2766-3.

Leamon, R. J., R. C. Canfield, S. L. Jones, K. Lambkin, B. J. Lundberg, and A. A. Pevtsov (2004), Helicity of magnetic clouds and their associated active regions, *J. Geophys. Res.*, 109, A05106, doi:10.1029/2003JA010324.

Lepping, R. P., D. B. Berdichevsky, C.-C. Wu, A. Szabo, T. Narock, F. Mariani, A. J. Lazarus, and A. J. Quivers (2006), A summary of WIND magnetic clouds for years 1995–2003: Model-fitted parameters, associated errors and classifications, *Ann. Geophys.*, 24, 215–245, doi:10.5194/angeo-24-215-2006.

Lopez, R. (1987), Solar cycle invariance in solar wind proton temperature relationships, *J. Geophys. Res.*, 92, 11,189–11,194, doi:10.1029/JA092iA10p11189.

Lynch, B. J., J. R. Gruesbeck, T. H. Zurbuchen, and S. K. Antiochos (2005), Solar cycle-dependent helicity transport by magnetic clouds, *J. Geophys. Res.*, 110, A08107, doi:10.1029/2005JA011137.

Marubashi, K. (1997), Interplanetary magnetic flux ropes and solar filaments, in *Coronal Mass Ejections*, Geophys. Monogr. Ser, vol. 99, edited by N. Crooker et al., pp. 147–156, AGU, Washington, D. C., doi:10.1029/GM099p0147.

Marubashi, K., and R. P. Lepping (2007), Long-duration magnetic clouds: A comparison of analyses using torus- and cylinder-shaped flux rope models, *Ann. Geophys.*, 25, 2453–2477, doi:10.5194/angeo-25-2453-2007.

Marubashi, K., S.-K. Sung, K.-S. Cho, and R. P. Lepping (2009), Impacts of torus model on studies of geometrical relationships between interplanetary magnetic clouds and their solar origins, *Earth Planets Space*, 61, 589–594.

Möstl, C., C. Miklenic, C. J. Farrugia, M. Temmer, A. Veronig, A. B. Galvin, B. Vršnak, and H. K. Biernat (2008), Two-spacecraft reconstruction of a magnetic cloud and comparison to its solar source, *Ann. Geophys.*, 26, 3139–3152, doi:10.5194/angeo-26-3139-2008.

Mulligan, T., C. T. Russell, and J. G. Luhmann (1998), Solar cycle evolution of the structure of magnetic clouds in the inner heliosphere, *Geophys. Res. Lett.*, 25, 2959–2962, doi:10.1029/98GL01302.

Romashets, R. P., and M. Vandas (2003), Force-free field inside a toroidal magnetic cloud, *Geophys. Res. Lett.*, 30(20), 2065, doi:10.1029/2003GL017692.

Schmieder, B., et al. (2011), Actors of the main activity in large complex centers during the 23 solar cycle maximum, *Adv. Space Res.*, 47, 2081–2091, doi:10.1016/j.asr.2011.02.001.

Shimazu, H., and M. Vandas (2002), A self-similar solution of expanding cylindrical flux ropes for any politropic index values, *Earth Planets Space*, 54, 783–790.

Shiota, D., K. Kusano, T. Miyoshi, and K. Shibata (2010), Magnetohydro-dynamic modeling for a formation process of coronal mass ejections: Interaction between an ejecting flux rope and an ambient field, *Astrophys. J.*, *718*, 1305–1314, doi:10.1088/0004-637X/718/2/1305.

Tripathi, D., V. Bothmer, and H. Cremades (2004), The basic characteristics of EUV post-eruptive arcades and their role as tracers of coronal mass ejection source region, *Astron. Astrophys.*, *422*, 337–349, doi:10.1051/0004-6361:20035815.

Vourlidas, A., R. Colaninno, T. Nieves-Chinchilla, and G. Stenborg (2011), The first observation of a rapidly rotating coronal mass ejection in the middle corona, *Astrophys. J. Lett.*, *733*, L23–L28, doi:10.1088/2041-8205/733/2/L23.

Wang, Y., G. Zhou, P. Ye, S. Wang, and J. Wang (2006), A study of the orientation of interplanetary magnetic clouds and solar filaments, *Astrophys. J.*, *651*, 1245–1255, doi:10.1086/507668.

Yurchyshyn, V. B., H. Wang, P. R. Goode, and Y. Deng (2001), Orientation of the magnetic fields in interplanetary flux ropes and solar filaments, *Astrophys. J.*, *563*, 381–388, doi:10.1086/323778.

Yurchyshyn, V., Q. Hu, and V. Abramenko (2005), Structure of magnetic fields in NOAA active regions 04486 and 0501 and the associated interplan-etary ejecta, *Space Weather*, *3*, S08C02, doi:10.1029/2004SW000124.

Yurchyshyn, V., V. Abramenko, and D. Tripathi (2009), Rotation of white-light coronal mass ejection structures as inferred from LASCO corona-graph, *Astrophys. J.*, *705*, 426–435, doi:10.1088/0004-637X/705/1/426.

Zhang, J., et al. (2007), Solar and interplanetary sources of major geomag-netic storms (Dst ≤ −100 nT) during 1996–2005, *J. Geophys. Res.*, *112*, A10102, doi:10.1029/2007JA012321.

K.-S. Cho, Y.-H. Kim, K. Marubashi, S.-H. Park, and Y.-D. Park, Korea Astronomy and Space Science Institute, 61-1 Whaam-dong, Yuseong-gu, Daejeon, 305-348, South Korea. (kmaru@kasi.re.kr)